Bulletin of Engineering Geology and the Environment (2024) 83:479
https://doi.org/10.1007/s10064-024-03975-5

ORIGINAL PAPER

Increasing accuracy in predicting mode I fracture toughness of rock structures: a comparative analysis of the rock engineering system method

Hadi Fattahi[1] · Hossein Ghaedi[1] · Danial Jahed Armaghani[2]

Received: 1 January 2024 / Accepted: 18 October 2024

Abstract
The investigation of crack initiation and expansion is vital for the stability of structures. The Mode I fracture toughness (K_{Ic}) of rocks is a key property used to predict crack propagation in tension and hydraulic fracturing. Various methods have been introduced to determine K_{Ic}, but results differ due to factors like sample dimensions, crack geometry, groove type, and loading conditions. The cracked chevron notched Brazilian disc (CCNBD) sample is commonly used in laboratory tests for its easy preparation. This study employs the rock engineering system (RES) technique to overcome the challenges of time-consuming and costly laboratory tests and the uncertainty in traditional methods (analytical, numerical, experimental, laboratory, regression). Using 88 CCNBD rock samples proposed by ISRM, input parameters include thickness of the disc specimen (B), uniaxial tensile strength (σ_t), initial crack length (α_0), radius of the disc specimen (R), crack length (α_B), and the length of the final crack (α_1). The RES-based model used 70 data points (80% of the dataset) for development, and 18 data points (20%) for evaluation. Regression analysis compared the performance of the RES method, using statistical indicators such as squared correlation coefficient (R^2), mean square error (MSE), and root mean square error (RMSE) to measure accuracy. The RES-based method outperformed other regression techniques, demonstrating significantly enhanced accuracy. This highlights the effectiveness and superior performance of the RES method in estimating fracture toughness, particularly for CCNBD samples, showcasing its potential as a robust analytical tool.

Keywords Crack initiation · Mode I fracture toughness · Rock structures · CCNBD · Rock engineering system

Introduction

Fracture toughness, also known as the critical stress intensity coefficient, is an inherent property of rock that represents its resistance to crack propagation or the amount of energy required to initiate a new crack.

Crack initiation and propagation in structures are crucial aspects of rock engineering and structural stability. Cracks, regardless of their size, significantly influence the strength and deformation of rock masses (Abe et al. 1976). These factors are pivotal for the stability of various structures such as open pits, underground mines, tunnels, and rock slopes. In the realm of energy reservoir exploration, rock fracturing plays a critical role by enhancing oil and gas production through the creation of new cracks (Funatsu et al. 2015). The determination of fracture toughness involves conducting various tests under both static and dynamic loading conditions, encompassing three primary failure modes: Mode I (tensile mode), where crack surfaces separate from each other; Mode II (shear mode), where crack surfaces slide relative to each other within the plane; and Mode III (tearing mode), where crack surfaces slide out of the plane without separation. Combined modes can also occur when two or all three loading modes act simultaneously. In rock mechanics, Mode I is particularly significant due to the brittle nature of rocks and their susceptibility to tension. Figure 1 illustrates different states of crack plate displacement (Ayatollahi and Akbardoost 2014; Mohammadi 2008; Preiß 2018; Saouma 2000).

✉ Danial Jahed Armaghani
danial.jahedarmaghani@uts.edu.au

[1] Faculty of Earth Sciences Engineering, Arak University of Technology, Arak, Iran

[2] School of Civil and Environmental Engineering, University of Technology Sydney, Sydney, NSW 2007, Australia

Published online: 04 November 2024

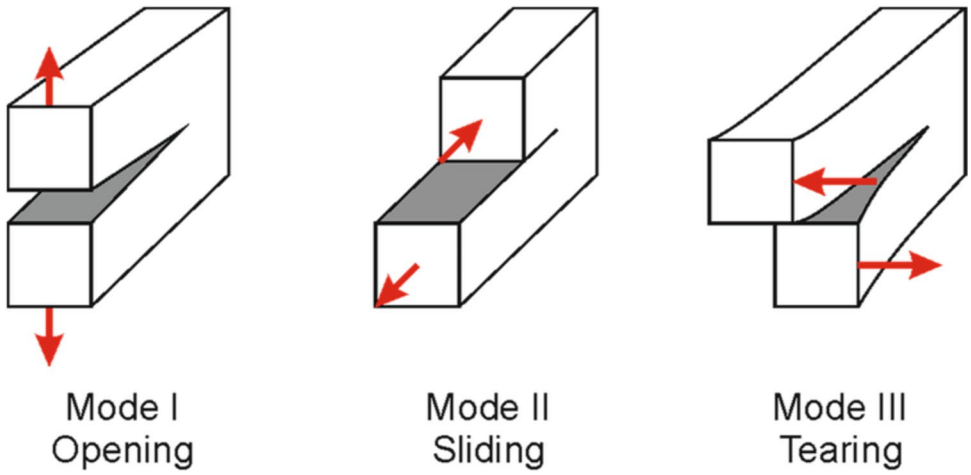

Fig. 1 Different states of crack plate displacement (Preiß 2018)

Several tests have been developed to determine Mode I fracture toughness (K_{Ic}) for rocks with a straight groove. These include tests using cylindrical samples with a straight groove (Ouchterlony 1981), disk samples with a straight groove (Alkılıçgil 2006; Tutluoglu and Keles 2011), semi-circular samples with a straight groove (the standard proposed by the International Society of Rock Mechanics in 2013) (Chong et al. 1987; Kuruppu et al. 2014; Lim et al. 1994), and the Brazilian specimen test with a straight groove (Fowell and Xu 1993). However, practical observations have shown discrepancies in fracture toughness values obtained from these tests. Numerous researchers have investigated fracture toughness in various rock types using diverse methodologies including analytical, numerical, experimental, and laboratory techniques. For instance, Schmidt and Huddle explored fracture toughness in Indiana limestone using SENB specimens under varying confining pressures, noting a substantial increase in K_{Ic} with higher pressure (Schmidt and Huddle 1977). Bearman (1999) established an empirical relationship between K_{Ic} and the point load index, while Bhagat (1985) conducted laboratory tests correlating K_{Ic} with tensile strength. Alkılıçgil (2006) utilized finite element software to study rock hardness, finding consistent results across different software programs (Abaqus, Ansys, Franc^{2D}, and Franc^{3D}). Wei et al. (2018b) compared CCNBD and CCNSCB rock samples, concluding higher toughness in CCNSCB samples, suitable for engineering applications. Funatsu et al. (2015) examined SCB and CB rock samples, observing different toughness values between Modes I and II. Wu et al. (2017) investigated the effect of confining pressure on K_{Ic} in granite, marble, and limestone, noting similar toughness responses across all rock types. Sun and Ouchterlony (1986) studied granite samples, finding varied toughness values among different sample types. Funatsu et al. (2015) also observed increased fracture toughness with higher confining pressure in Kimachi sandstone and tuff. Ma et al. (2021) addressed the failure mechanisms in roof layers of Dongjiahe coal mine using microseismic moment tensor analysis, while Liu et al. (2024) used 3D Discontinuous Deformation Analysis (DDA) to study rock slope wedge failure mechanisms and damage characteristics. Similarly, Liu et al. (investigated rockfall using 3D DDA, assessing damage areas and movement ranges. Ma and Liu (2022) conducted comprehensive research on rockfall mechanisms and mitigation using the 3D DDA method. Despite the valuable insights gained from these studies on fracture toughness, variations in rock properties across different locations introduce uncertainties and limit accuracy. Addressing these challenges, recent efforts employ intelligent methods and algorithms to better account for uncertainties in rock engineering and fracture toughness (Afrasiabian and Eftekhari 2022; Daghigh et al. 2020; Dehestani et al. 2022; Emami Meybodi et al. 2022; Fakhri et al. 2022; Hamdia et al. 2015; Mahmoodzadeh et al. 2023, 2022; Mazhnik and Oganov 2020; Roy et al. 2018).

In mining and civil engineering, understanding stability, crack propagation, and failure mechanisms is crucial for minimizing hazards and financial losses. Accurately predicting K_{Ic} plays a vital role in achieving this objective. However, the complexities and variability of rock parameters pose challenges that require methods capable of capturing complex interactions among geological factors. The RES (Rock Engineering Systems) method addresses these challenges by incorporating diverse rock parameter values, prioritizing and ranking them based on expert opinions in rock engineering. Unlike traditional methods, RES effectively manages uncertainties in rock parameters through its matrix-based approach, which simplifies the integration of expert judgments. Moreover, RES offers several advantages: it requires no complex coding, facilitating easy modeling in Excel; it performs complex and nonlinear modeling swiftly and with high accuracy compared to regression methods; and it can model multiple case studies if parameters are similar. Another notable advantage of RES is its flexibility

to quickly adapt modeling to changes in input parameters or additional analyses. This flexibility, coupled with its ability to provide precise predictions and optimize resource allocation, underscores its competitive edge. The method's application to analyzing CCNBD samples in laboratory research not only mitigates challenges for engineers and practitioners but also ensures project execution with accuracy and efficiency. The cost-effectiveness and compatibility of RES position it as a compelling alternative to traditional methodologies in the field.

Based on the topics discussed, the main objective of this paper is to apply the RES-based method for estimating K_{Ic} in CCNBD rock samples as defined by ISRM standards. The RES method offers significant advantages such as simplicity, cost-effectiveness, time efficiency, and the capability to handle rock parameter uncertainties without the need for intricate coding. By leveraging the RES method, precise predictions of fracture toughness can be achieved across various rock samples.

The RES-based method has been employed in various studies for a range of applications. These include:

- Assessing and forecasting rock fragmentation and crushing hazards resulting from explosions at the Songon open-pit copper mine in East Azarbaijan province, Iran (Hasanipanah et al. 2016).
- Determining maximum ground surface settlement resulting from underground space excavation using TBM-EPB machines (Fattahi and Babanouri 2018).
- Assessing the likelihood of underground coal mine fires triggered by explosions (Saffari et al. 2013).
- Estimating the explosion potential in underground coal mines due to gas presence between coal seams (Zhou et al. 2019).
- Assessing surface settlement, distortion, and structural damage resulting from drilling with TBM machines (Mohammadi and Azad 2021).
- Analyzing safety parameters' impact on risks associated with circular slope failures (Fattahi 2017).
- Predicting changes in deformation modulus of rock mass (Fattahi and Moradi 2018).
- Forecasting TBM-EPB machine penetration rates in underground excavations (Frough and Torabi 2013).
- Estimating methane gas release potential in underground coal mines (Ghanbari et al. 2018).

These applications highlight the versatility and effectiveness of the RES-based method in tackling various challenges within mining and civil engineering contexts.

In this particular study, the K_{Ic} was estimated using the RES-based method for 88 CCNBD rock samples proposed by ISRM. To validate the constructed model using the RES-based method, statistical indicators such as the squared correlation coefficient (R^2), mean square error (MSE), and root mean square error (RMSE) were employed.

Crack chevron notch brazilian disk (CCNBD)

In 1995, the International Society of Rock Mechanics (ISRM) introduced the CCNBD sample, depicted in Fig. 2, as a tool for assessing the fracture toughness of rock samples. This approach facilitates a comprehensive examination of fracture mechanisms across Mode I, Mode II, and combined modes.

Furthermore, as shown in Fig. 2, the dimensionless parameters α_0, α_1, α_B and α_S in the ISRM's CCNBD samples can be defined using the following relationships:

$$\alpha_0 = \alpha_0/R \tag{1}$$

$$\alpha_0 = \alpha_1/R \tag{2}$$

$$\alpha_B = B/R \tag{3}$$

$$\alpha_S = R_S/R \tag{4}$$

In these equations, α_0 represents the initial crack length, R is the radius of the disc specimen, α_1 denotes the final crack length, α_B is the crack length, B represents the thickness of the disc specimen, α_S indicates the length of the chevron saw gap (created by a two-blade cut), R_s is the gap resulting from the radius of the chevron saw's two-blade cut, and P represents the applied pressure on the CCNBD sample.

In certain cases, the two-dimensional strain mode used to assess the toughness and fracture behavior of CCNBD samples may not fully capture the results for all rock geometries. Previous studies have suggested limiting the geometry of rock samples within the range illustrated in

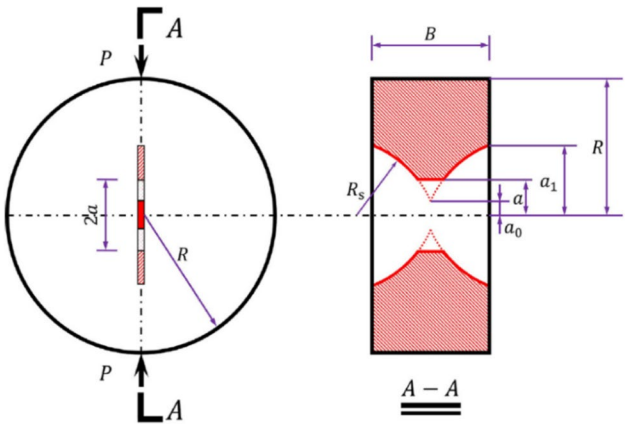

Fig. 2 Geometrical characteristics of the CCNBD test(Wang et al. 2021)

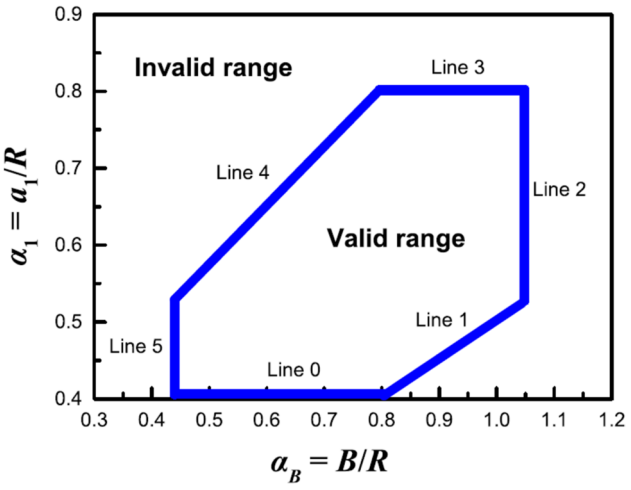

Fig. 3 Permissible range for calculating K_{Ic} in the ISRM's proposed tests (Wang et al. 2021)

Fig. 3 to accurately measure the toughness for various rock types (Fowell and Xu 1993; Fowell et al. 2006).

Mathematically, this can be expressed as follows:

$$\alpha_1 \geq 0.4 \text{ Line 0} \tag{5}$$

$$\alpha_1 \geq \alpha_B/2 \text{ Line 1} \tag{6}$$

$$\alpha_B \leq 1.04 \text{ Line 2} \tag{7}$$

$$\alpha_1 \leq 0.8 \text{ Line 3} \tag{8}$$

$$\alpha_B \geq 1.1729.(\alpha_1)^{5/3} \text{ Line 4} \tag{9}$$

$$\alpha_B \geq 0.44 \text{ Line 5} \tag{10}$$

The K_{Ic}, denoted as kI, can be expressed by considering the fracture mechanism as linear elastic for CCNBD rock samples (Fowell et al. 2006; Xu et al. 2016).

$$k_I = \frac{P_{\max}}{B.\sqrt{R}}.Y^*_{\min} \tag{11}$$

In the above equation, P_{max} represents the maximum pressure applied to the CCNBD sample, which Y^*_{min} is obtained from the following equation (Fowell et al. 1995, 2006).

$$Y^*_{\min} = ue^{va_1} \tag{12}$$

Here, the constant parameters u and V are determined based on the values of α_0 and α_B (Aliha and Ayatollahi 2014).

Database

Constructing a robust model using the RES method requires a significant amount of data that includes the actual input and output parameters obtained from the CCNBD test samples suggested by ISRM. To accomplish this, a combination of laboratory test data and numerical modeling results from previous studies were utilized (Aliha et al. 2006; Aliha and Ayatollahi 2014; Cui et al. 2010; Wei et al. 2018a, 2018b). It should be noted that since numerical software accepts only one value for rock properties, multiple modeling iterations were conducted in previous studies.

In this study, CCNBD samples used for laboratory testing were derived from Dazhou sandstone, possessing an average Young's modulus of 16.5 GPa and a Poisson's ratio of 0.22. Mineral composition analysis by X-ray diffractometer revealed quartz, clathrasil, and silicon iron carbide as comprising 88%, 4%, and 3% of the rock material, respectively. The preparation of specimens followed meticulous ISRM-suggested procedures, ensuring geometric parameters met dimensional requirements necessary for valid tests (Fowell 1995). Additionally, to assess the fracture toughness of rock structures, coarse-grained white marble named Marmarharsin from Kermanshah province, Iran, was utilized. This marble is characterized as a homogeneous material with minimal discontinuities, facilitating analysis under consistent and uniform conditions.

In the course of this research, a comprehensive dataset of 88 data points was employed, inclusive of both experimental observations from laboratory tests and numerical modeling outcomes for CCNBD test samples recommended by ISRM. Constructing the model using the RES method involved a random selection of 80% of the dataset (70 data points) for the initial model development, with the remaining 20% (18 data points) dedicated to the critical phase of model verification. This meticulous approach ensures the robustness and reliability of the model by assessing its performance against a distinct set of data points. The input parameters considered in this study include uniaxial tensile strength (σ_t (MPa)), initial crack length (α_0), radius of the disc specimen (R(mm)), crack length (α_B), thickness of the disc specimen (B(mm)), and final crack length (α_1). The output parameter in this study is the K_{Ic}, which serves as the model's prediction. Table 1 showcases a segment of the data that has been utilized and discussed in detail within this paper (Aliha et al. 2006, 2018; Aliha and Ayatollahi 2014; Cui et al. 2010; Wei et al. 2018a, 2018b).

Descriptive statistics for both the output and inputs data, including maximum, minimum, mean, mode, median, range, and standard deviation, are provided in Table 2.

Table 1 A subset of the inputs and output data used to construct the model (Wang et al. 2021)

No	Inputs						Output
	σ_t (Mpa)	**R(mm)**	**B(mm)**	**α_B**	**α_0**	**α_1**	**K_{Ic} (Mpa.$\sqrt{m}$)**
1	13.2	24.9	19.76	0.794	0.297	0.723	1.4
2	13.2	24.9	19.62	0.788	0.321	0.727	1.63
3	13.2	24.9	19.8	0.795	0.273	0.719	1.44
4	13.2	24.9	19.62	0.788	0.249	0.715	1.69
5	13.2	24.9	19.8	0.795	0.361	0.735	1.47
6	13.2	24.9	20.06	0.806	0.289	0.727	1.71
7	13.2	50.1	40	0.798	0.333	0.725	1.73
8	13.2	50.1	40	0.798	0.253	0.715	1.59
9	13.2	50.1	40	0.798	0.253	0.715	1.72
10	13.2	50.1	40	0.798	0.222	0.709	1.71

Table 2 Descriptive statistics for both the output and inputs data

Type	Parameters	Max	Min	Mode	Mean	Std. Deviation	Range	Median
Inputs	σ_t (Mpa)	16.10	4.60	16.10	10.3511	5.11345	11.5	13.2
	R (mm)	75.25	24.90	38	42.1088	13.08190	50.35	38
	B (mm)	60	17.88	30	29.9609	9.73261	42.12	29.2
	α_B	0.8575	0.545	0.79	0.7201	0.09959	0.31	0.7675
	α_0	0.393	0.211	0.26	0.2693	0.03324	0.18	0.261
	α_1	0.742	0.604	0.65	0.6792	0.04369	0.14	0.698
Output	K_{IC} (Mpa.$\sqrt{m}$)	3.325	0.4905	1.07	1.4734	0.71771	2.83	1.213

To enhance the understanding of the descriptive statistics presented in Table 2, graphical representations were utilized. Therefore, Fig. 4 displays a box plot generated by SPSS software for the data in Table 2.

A box plot is a standard method for visualizing data distribution using key statistical indicators: first quartile (Q_1), Minimum value, median, Maximum value and third quartile (Q_3). It also helps identify outliers, which are crucial in data analysis as they can potentially skew results if not accounted for. In Fig. 3, the interquartile ranges of parameters B, α_1 and α_B, α_0 are observed to be smaller compared to other parameters. This indicates that these data sets are more concentrated and have less dispersion. Additionally, the absence of outliers in the data depicted by the figure ensures that the analysis results will not be influenced in an erroneous direction by various statistical methods.

The correlation between parameters, a crucial statistical indicator, highlights their relationship. A negative correlation indicates an inverse relationship, whereas a positive correlation signifies a direct connection. Understanding these correlations is pivotal in statistical analysis. The strength of correlation, whether positive or negative, is measured on a scale from 0 (weak correlation) to 1 (strong correlation). Figure 5 illustrates the correlation between input and output parameters based on the data used in this study (88 data points). Based on the figure, the correlations between the input data variables among themselves and with the output variable are pairwise and symmetrical. For instance:

- The correlation between input variables R and B is the highest, at 0.87.
- The correlation between input variables B and σ_t is the lowest, at 0.09.
- The correlation between input variable R and the output variable K_{Ic} is 0.08, indicating a low correlation.
- Conversely, the correlation between input variable σ_t and the output variable K_{Ic} is higher, at 0.61.

These correlation coefficients provide insights into the relationships between the variables, highlighting stronger and weaker associations that are essential for understanding the data dynamics and informing subsequent analyses.

The primary objective of this paper is to develop a highly robust model using the RES-based method. Additionally, traditional regression analysis has been employed for performance comparison. This dual approach aims to highlight the advantages and improvements offered by the RES method over conventional regression techniques in modeling and prediction tasks. An overview of the model's design is depicted in Fig. 6.

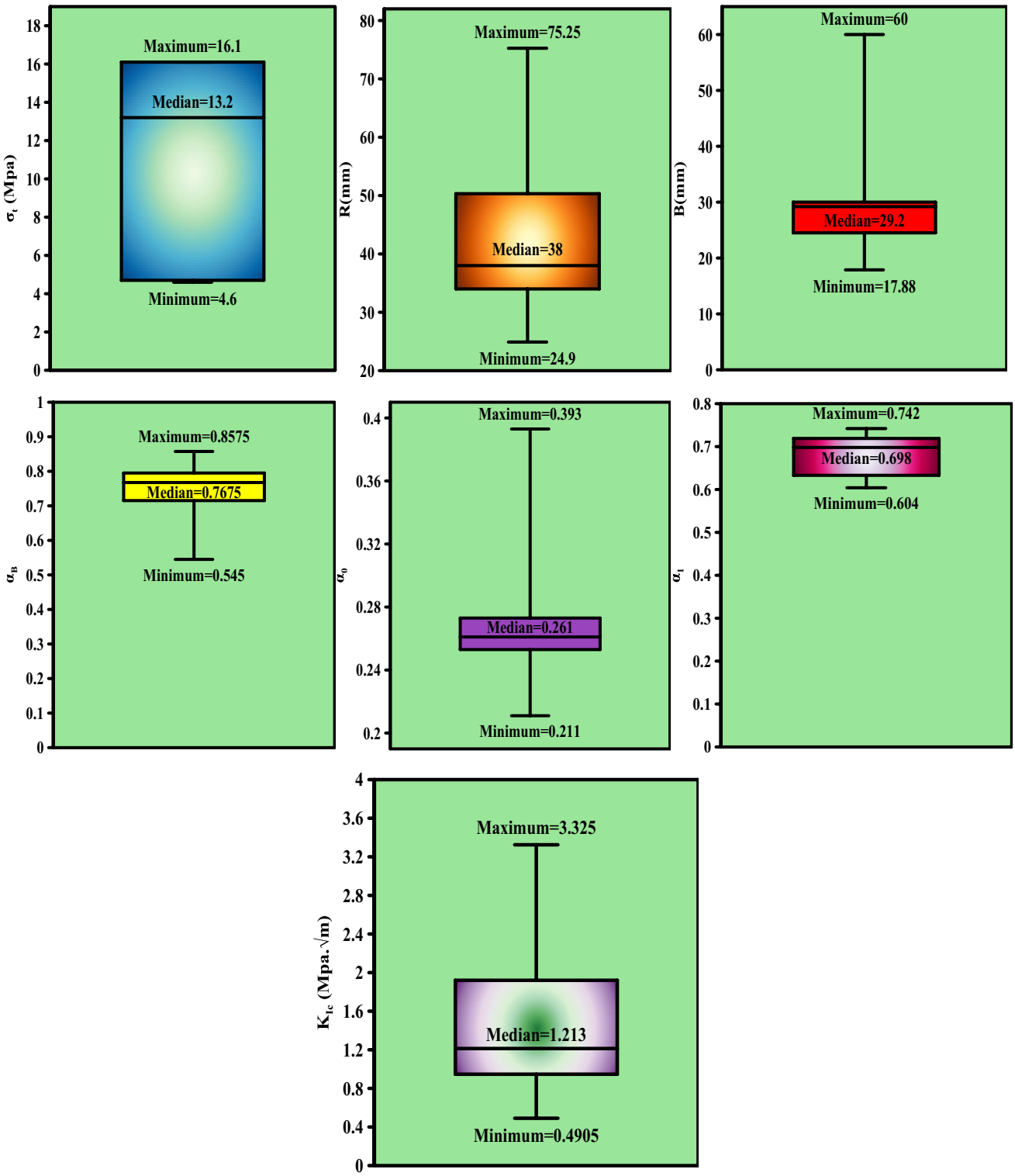

Fig. 4 Box plot of the data

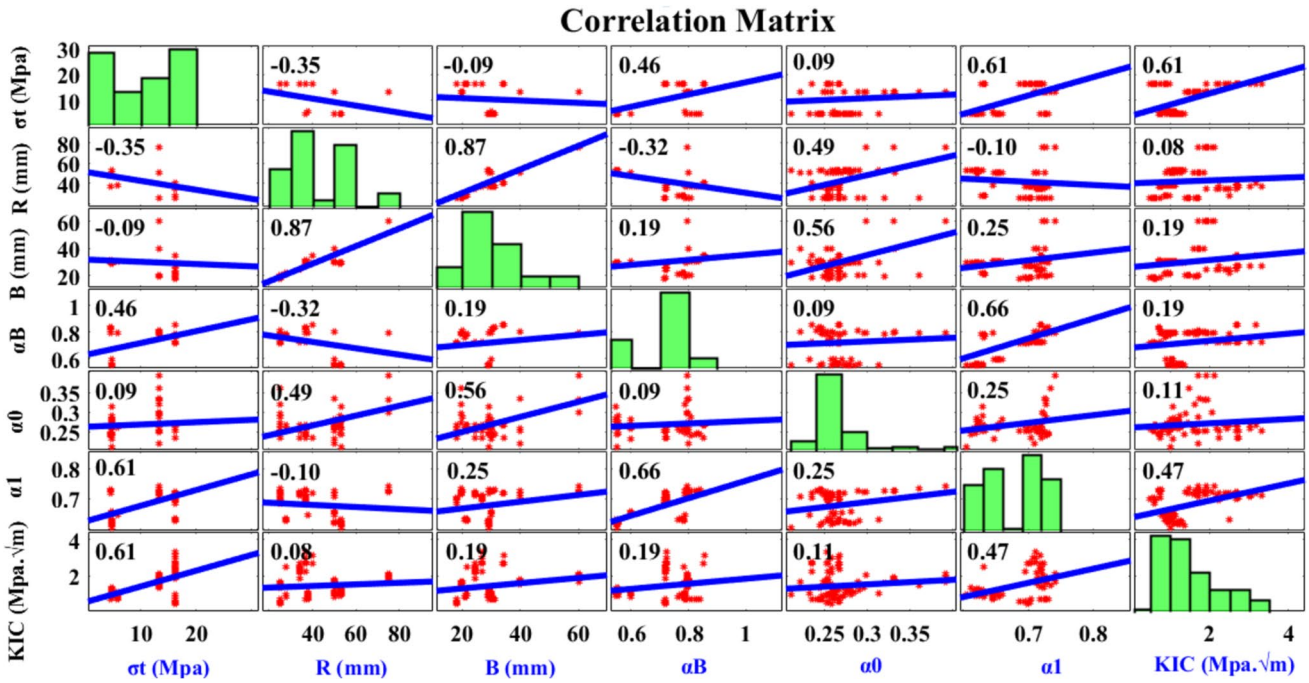

Fig. 5 Relationship between inputs and output data

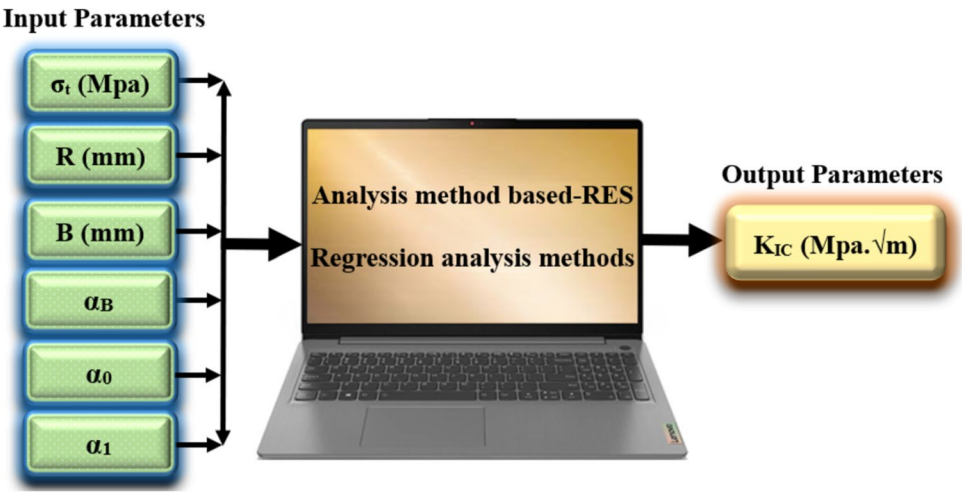

Fig. 6 Architecture of regression models and the RES-based method

Statistical modeling

Multiple linear regression analysis (MLR)

If there exists a multiple linear relationship between the input parameters and the dependent parameter (output of the model), the mathematical equation can be represented as follows:

$$y = W_1 + W_2x_2 + W_3x_3 + \cdots + W_nx_n + e \quad (13)$$

In Eq. (13), the variables are defined as follows: y represents the dependent variable, x denotes the independent variables or input parameters, e signifies the error term in the relationship, and W_1, W_2, W_3, …W_n are the coefficient values that can be determined through various methods, including the utilization of statistical software. Ensuring a high level of accuracy necessitates formulating an equation that demonstrates a robust convergence around the regression line. Conversely, when there is notable divergence and dispersion along the regression line, the accuracy of the constructed

model diminishes significantly. In this particular study, the focus was on multiple linear regression analysis conducted through SPSS statistical software, utilizing input parameters such as σ_t *(MPa), R (mm), B (mm),* α_B, α_0 and α_1. The equation for multiple linear regression analysis is presented below as part of the comprehensive exploration of the relationships within the dataset.

$$K_{Ic}(MPa.\sqrt{m}) = -13.847 + 0.122\sigma_t(MPa) + 0.269R(mm) + 0.32B(mm) + 14.385\alpha_B - 2.036\alpha_0 + 4.469\alpha_1 \quad (14)$$

To assess the presence of multicollinearity in the multiple linear relationship, a detailed multicollinearity analysis was conducted. The variance inflation factor (VIF) was utilized for this purpose, as it is a widely accepted measure for detecting multicollinearity among the predictor variables. VIF values can range from 1 to infinity, where a VIF value exceeding 10 typically indicates significant multicollinearity, suggesting that the predictor variables are highly correlated with each other (Seber and Lee 2003). High multicollinearity can inflate the variance of the coefficient estimates and make the model unstable. In this study, the VIF values for the input parameters in linear Eq. (14) were meticulously computed and presented in Table 3. By examining these VIF values, the study ensures that the predictors used in the model do not exhibit problematic multicollinearity, thus maintaining the reliability and accuracy of the model's predictions and interpretations.

Table 4 displays the results of the regression analysis for Eq. (14) and the ANOVA conducted in this study. The F-value and significance (Sig.) are critical in determining whether to reject the null hypothesis of no effect. In this study, the calculated F-value is 12.037, and the associated Sig. value is 0.000, which is less than the conventional threshold of 0.05. This low Sig. value strongly supports rejecting the null hypothesis, indicating a statistically significant impact of the studied variables on the dependent variable. The ANOVA results provide robust evidence that the regression model fits the data well and that the included variables collectively explain a significant portion of the variance in the dependent variable. These findings underscore the validity and reliability of the regression model based on Eq. (14), affirming its utility in predicting outcomes related to the studied phenomenon. This statistical validation enhances confidence in the model's ability to accurately represent and interpret the relationships among the variables under investigation.

Table 4 ANOVA for Eq. (14)

	Sum of squares	*df*	Mean square	*F*	Sig
Regression	21.449	6	3.575	12.037	0.000
Residual	18.710	63	0.297		
Total	40.159	69			

Multivariate regression models

In addition to linear regression analysis, this study utilized SPSS statistical software to perform polynomial, exponential, logarithmic, and power regression analyses for estimating K_{Ic} (model output). These analyses employed the same input data and parameters as those in the multiple linear regression analysis, ensuring consistency in the evaluation process. The results of these regression analyses provided different functional forms to describe the relationship between the input variables and the output variable, K_{Ic}. Each regression model was evaluated based on its R^2, which quantifies the proportion of variance in K_{Ic} explained by the model. These R^2 values serve as indicators of how well each regression model fits the data and elucidate the strength of the relationship captured by each functional form. By examining and comparing the outcomes of these various regression techniques, the study aimed to identify the most suitable model for accurately predicting K_{Ic} and to gain insights into

Table 3 Information about the input parameters of the multiple linear Eq. (14)

Independent variables	Unstandardized coefficients		Standardized coefficients β	95.0% Confidence interval for *B*		Collinearity statistics		t values	R^2	Standard error of estimate
	B	**Std.error**		**Lower Bound**	**Upper Bound**	**Tolerance**	**VIF**			
Constant	-15.607	5.172		-25.942	-5.271			-3.018	0.954	0.54496
σ_t (Mpa)	0.12	0.019	0.830	-0.159	-0.082	0.419	2.388	6.248		
R (mm)	0.288	0.097	4.452	-0.481	-0.094	0.107	9.34	2.970		
B (mm)	-0.345	0.126	-3.822	0.093	0.597	0.101	9.9	-2.737		
α_B	15.291	6.022	1.936	3.256	27.326	0.12	8.33	2.539		
α_0	-2.185	3.173	-0.063	-8.526	4.157	0.870	1.149	-0.688		
α_1	5.373	2.289	0.3	0.8	9.947	0.454	2.202	2.348		

the nature of the relationship between the input parameters and the fracture toughness parameter K_{Ic}.

The polynomial model with $R^2 = 0.3452$, is represented as:

$$K_{Ic}\,(MPa.\sqrt{m}) = -2.137 - (-0.14\sigma_t(MPa)) + (0.001R(^m) + (3{,}804\alpha_B{}^4) + (28.282\alpha_0{}^5) + (6.097\alpha_1{}^6) \quad (15)$$

The exponential model with $R^2 = 0.2592$ is given by:

$$K_{Ic}(MPa.\sqrt{m}) = -6.727 - 0.00000007554exp(\sigma_t(MPa)) - 4.7E-25exp(R(mm)) + 1.97E-18exp(B(mm)) - 0.888exp(\alpha_B) + 2.935exp(\alpha_0) + 2.985exp(\alpha_1) \quad (16)$$

The logarithmic model with $R^2 = 0.6788$ is expressed as:

$$K_{Ic}(MPa.\sqrt{m}) = -5.026 + 0.986ln(\sigma_t(MPa)) - 1.413ln(R(mm)) + 2.606ln(B(mm)) - 3.355ln(\alpha_B) - 0.527ln(\alpha_0) + 2.626ln(\alpha_1) \quad (17)$$

The power model with $R^2 = 0.8281$ can be written as:

$$K_{Ic}(MPa.\sqrt{m}) = 10^{-8.968+0.057\sigma_t(MPa)+0.16R(mm)-0.199B(mm)+8.089\alpha_B-0.95\alpha_0+3.13\alpha_1} \quad (18)$$

Table 5 Explanations for classifying the intensity of parameter interactions (Hudson 1992)

Code number	Intensity of parameter interactions
4	Intense
3	High
2	Moderate
1	Low
0	No

Rock engineering system (RES)

Identifying and influencing the parameters that affect models related to rock engineering problems has always been challenging and complex. In 1992, Hudson introduced the concept of RES for the first time (Hudson 1992). The RES method involves three steps: identifying the parameters and factors that influence the model's output, creating an interaction matrix for these parameters, and ranking them. Due to the difficulty of determining the interdependencies between parameters, the RES method utilizes the interaction matrix to organize and describe the parameter relationships within the system. The interaction matrix strategically places crucial parameters influencing the system along the main diagonal, emphasizing their individual significance. Outside the main diagonal, the visual representation captures the effects of one parameter on another, showcasing the intricate relationships and dependencies within the system. This matrix design facilitates a clear and structured understanding of how specific elements interact and impact each other within the larger system.

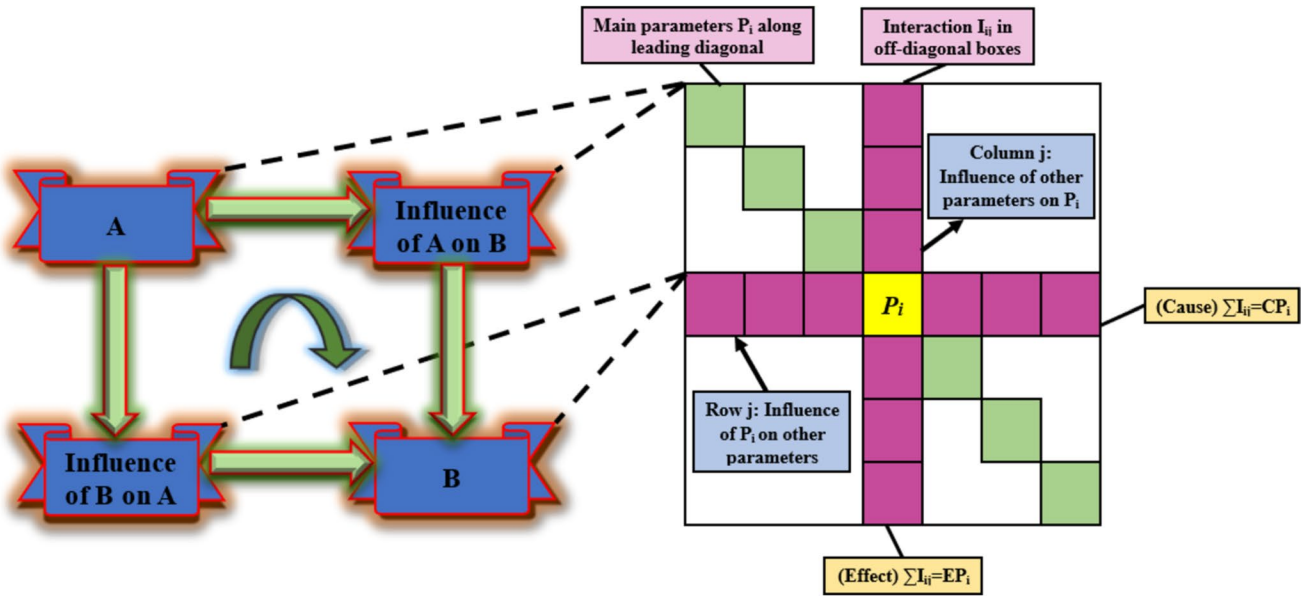

Fig. 7 The functioning of the interaction matrix in the RES method (Hudson 1992)

Figure 7 illustrates the clockwise functioning of the interaction matrix.

Various methods exist for coding the interactions outside the main diagonal. One practical, simple, and effective coding method is the expert semi-quantitative (ESQ) method introduced by Hudson (1992). Interactions in this coding method are rated on a scale from 0 to 4 to signify their varying degrees or intensities. A value of 0 indicates no interaction, while a value of 4 represents a very strong interaction. Table 5 provides additional explanations for classifying the intensity of parameter interactions.

Upon encoding the interaction matrix, the sum of the row values, referred to as cause (C), delineates the collective effect of each parameter on the system. This sum quantifies how much each parameter influences the overall dynamics of the system. Conversely, the sum of column values, referred to as influence (E), elucidates the system's impact on individual parameters. The mathematical expressions for cause and effect are as follows:

$$C_{pi} = \sum_{j=1}^{n} I_{ij} \tag{19}$$

$$E_{pi} = \sum_{i=1}^{n} I_{ij} \tag{20}$$

Based on the cause and effect values obtained from Eqs. (19) and (20), the intensity and dominance of parameters can be determined by summing and subtracting cause and effect ($C+E$, C-E). Additionally, the weighting factor (a_i) can be calculated using cause and effect values according to Eq. (21) (Benardos and Kaliampakos 2004).

Estimating K_{Ic} and risk assessment using the RES method

The Vulnerability Index (VI) approach is a fundamental factor in assessing risk levels and estimating model outputs. VI was initially introduced to investigate and evaluate geological and geotechnical risks during tunnel excavation using a TBM machine. This method helps identify potential hazards and ensures the safety and efficiency of the tunneling process. In this paper, the VI index is used to estimate, predict, and assess the risk level of K_{Ic}. To accomplish this, three steps should be followed:

Step 1: Identify all important parameters influencing K_{Ic}. Evaluate the weight or intensity of influence of each parameter in the risk analysis. The principles of the RES method provide a valuable framework for assessing and establishing the significance of individual parameters in influencing the model's output.

Table 6 Classification of VI based on risk level (Benardos and Kaliampakos 2004)

Risk description	High to very high	Medium to high	Low to medium
VI	66–100	33–66	0–33
Category	III	II	I

Table 7 The input parameters that influence the model's output in the RES methodology

P_n	Parameter	Symbol
P_1	Uniaxial tensile strength	σ_t (MPa)
P_2	Radius of the disc specimen	R (mm)
P_3	Thickness of the disc specimen	B (mm)
P_4	Crack length	α_B
P_5	Initial crack length	α_0
P_6	Final crack length	α_1

Step 2: To build the model and assign risk levels, obtain the VI values for all parameters influencing the model. These values help prioritize parameters based on their impact on the model's output and facilitate the assessment of risk levels associated with each parameter. Equation (22), based on the VI proposed by Benardos and Kaliampakos (2004), is used for this purpose.

$$VI = 100 - \sum_{i=1} a_i \frac{Q_i}{Q_{\max}} \tag{21}$$

In Eq. (22), Q_{max} signifies the maximum parameter value or rating, Q_i represents the value of each individual parameter, and ai denotes the weight associated with the ith parameter, calculated from the equation. Table 6 provides a breakdown of the vulnerability index, categorized according to different risk levels. The vulnerability index is classified into three tiers: low to medium (optimal conditions), medium to high, and high to very high (critical conditions). This classification scheme aids in assessing and interpreting the vulnerability of the system based on the assigned risk levels (Benardos and Kaliampakos 2004).

Step 3: With the VI values obtained, it is possible to estimate K_{Ic}.

Risks and parameters related to K_{Ic}

Asmentioned earlier, one of the crucial steps in the RES method for modeling the system's output is identifying important and influential parameters. Table 7 presents the

Table 8 Interactions between parameters affecting the model's output

P_1	0	0	2	2	2
1	P_2	1	1	0	1
3	0	P_3	3	3	3
2	0	0	P_4	0	0
2	0	0	1	P_5	0
2	0	0	0	0	P_6

key variables and parameters that have the greatest impact on K_{Ic}.

Interaction matrix

This study strategically positions six pivotal parameters (P_1, P_2, P_3, P_4, P_5, P_6) as variables or input parameters along the main diagonal of the matrix. This arrangement emphasizes their individual significance in the context of the analyzed system. The ESQ method introduced by Hudson in 1992 is used to determine the effect of each of these parameters on the others outside the main diagonal. Based on expert opinions from rock mechanics experts, mining engineers, and geotechnical engineers, the interaction matrix presented in Table 8 is obtained.

Following Table 8, the cause and effect values obtained from summing the rows and columns of the interaction matrix are transferred to the coordinate axis. Figure 8 illustrates the placement of parameters based on cause (C) and effect (E). Parameters P_4 and P_6 (α_B, and α_1) have the greatest impact on the system and are located above the C = E line, indicating that they are influenced by the system. Parameters P_1, P_2, P_3 and P_5 (σ_t, B, R, α_0) are completely influenced by the system as they are below the C = E line.

Table 9 Weighting of key variables for K_{Ic}

Main factor	C	E	C-E	C+E	a_i (%)
σ_t (MPa)	6	10	-4	16	27.5862
R (mm)	4	0	4	4	6.89655
B (mm)	12	1	11	13	22.4138
α_B	2	7	-5	9	15.5172
α_0	3	5	-2	8	13.7931
α_1	2	6	-4	8	13.7931
Total	29	29	0	58	100

The effect (E), cause (C), dominance (C-E), interaction intensity (C + E), and weights of each parameter (ai) are presented in Table 9.

From Table 9, it can be concluded that the parameter P_1 (uniaxial tensile strength) has the greatest effect on K_{Ic}. A slight variation in uniaxial tensile strength exerts the

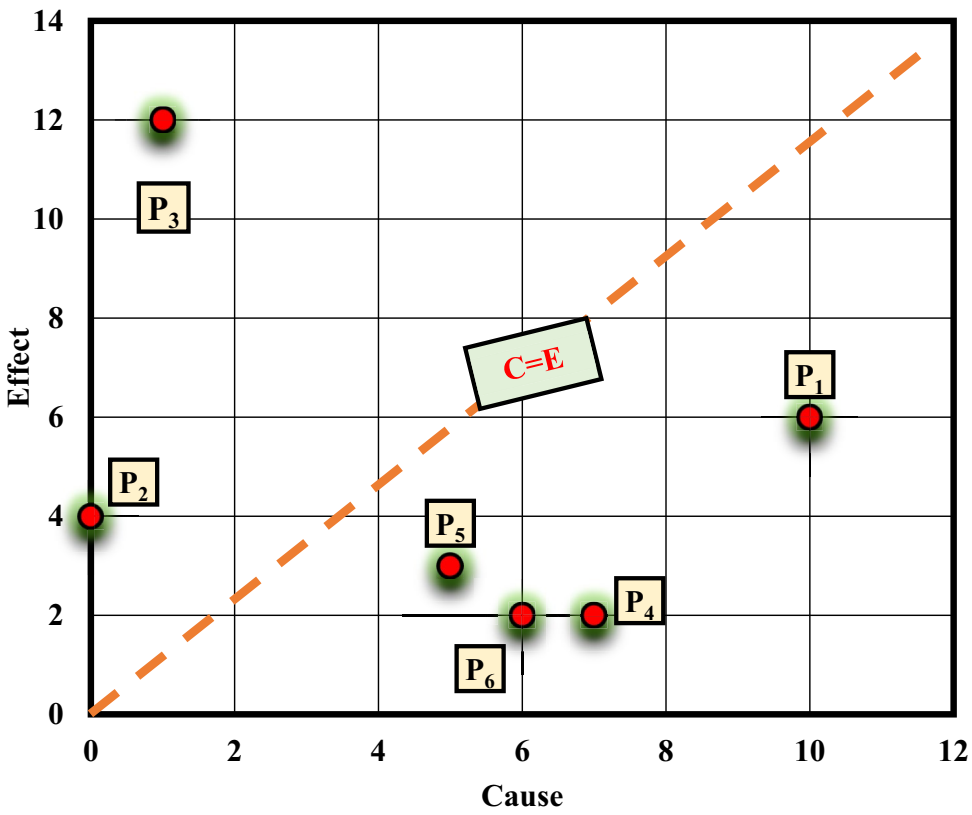

Fig. 8 Cause-Effect Plot for Principal Parameters of K_{IC}

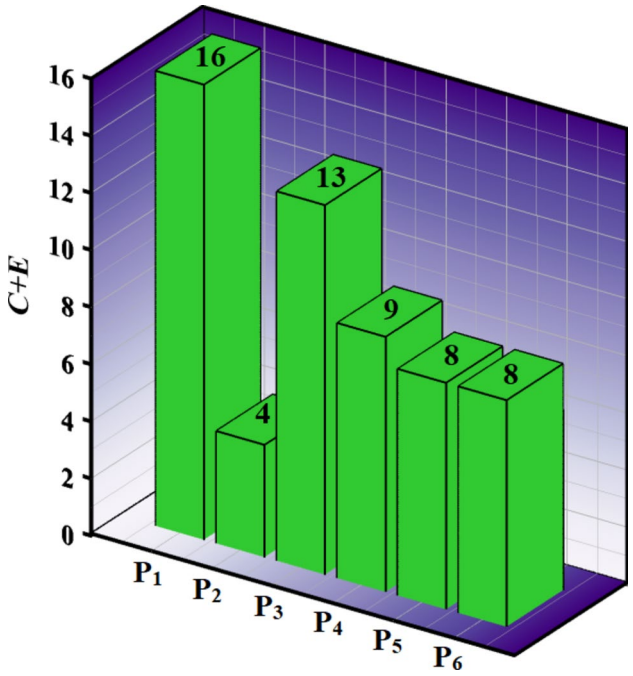

Fig. 9 Histogram Chart for Cause + Effect of Important Parameters of K_{Ic}

greatest influence on the model's output. Parameters with substantial effects on the system are referred to as unstable parameters. The histogram of interaction intensity, calculated as C + E, is depicted in Fig. 9.

Rating of parameters

To build the model, VI values need to be obtained. According to Eq. (22), the Q_i/Q_{max} values must be calculated first. Table 10 classifies and ranks the parameters affecting the model's output based on their values. The rating scale ranges from 0 to 4, with 0 indicating a negative parameter or the worst state, and 4 representing a positive parameter or the best state. In this study, input parameters were ranked based on evaluations from experts and engineers specializing in rock engineering.

Risk analysis and estimation of K_{Ic}

In this research, a substantial subset of the dataset, comprising 70 out of 88 data points (constituting 80% of the data), was employed to calculate the Vulnerability Index (VI) for constructing the model. The remaining 18 data points (20% of the data) played a crucial role in assessing and validating the model's performance. The specifics of the VI values for data point number 1 are detailed in Table 11, providing a comprehensive insight into the model's evaluation and validation process.

To better understand the significance of this analysis, Fig. 10 illustrates the VI values for all 70 data points. The average VI is 10, indicating a low to medium risk levelaccording to Table 6.

Table 10 Rating and values of input parameters

Number	Parameters	Values and Ratings					
1	σ_t (MPa)	Value	0–4.8	4.8–7	7–10	10–13	13 >
		Rating	0	1	2	3	4
2	R (mm)	Value	0–28	28–32	32–34	34–55	55 >
		Rating	0	1	2	3	4
3	B (mm)	Value	0–18	18–19.5	19.5–21.587	21.587–34	34 >
		Rating	0	1	2	3	4
4	α_B	Value	> 0.86	0.797–0.86	0.76–0.797	0.596–0.760	0–0.596
		Rating	0	1	2	3	4
5	α_0	Value	> 0.322	0.253–0.322	0.245–0.253	0.211–0.245	< 0.211
		Rating	0	1	2	3	4
6	α_1	Value	> 0.752	0.742–0.752	0.727–0.742	0.631–0.727	0–0.631
		Rating	0	1	2	3	4

Table 11 Details of the VI values for data point number 1

Parameters	σ_t (MPa)	R (mm)	B (mm)	α_B	α_0	α_1
Value or description	13.2	24.9	19.76	0.794	0.297	0.723
Value rating (Q_i)	4	0	2	2	1	3
Weighting (% a_i)	27.5862	6.89655	22.4138	15.5172	13.7931	13.7931
VI	39.65517					

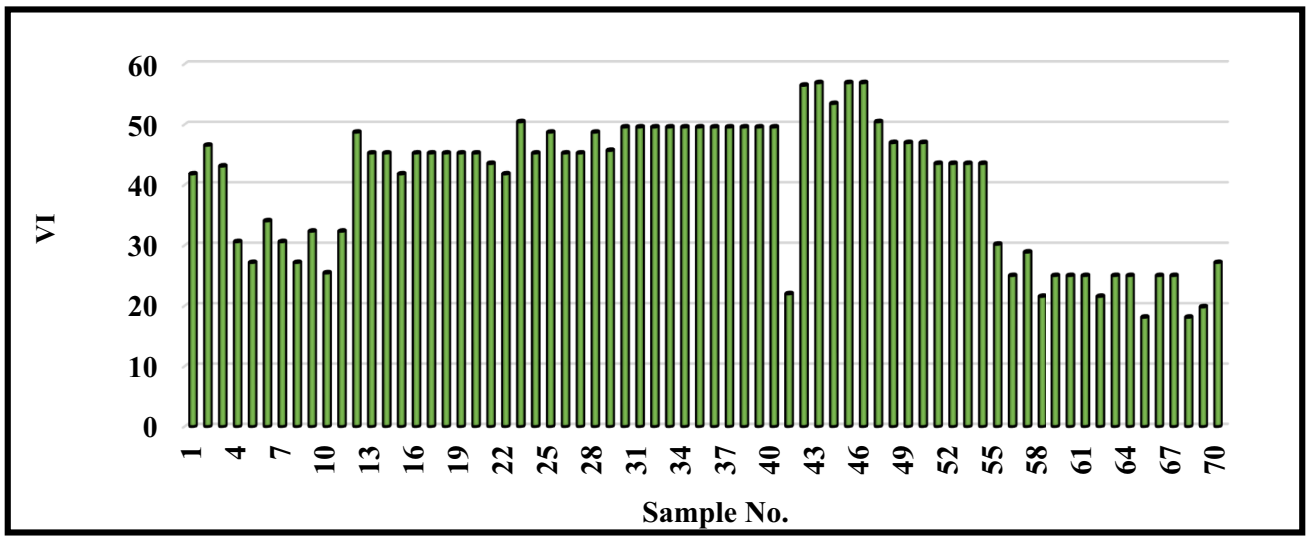

Fig. 10 VI for the Sample Data Points

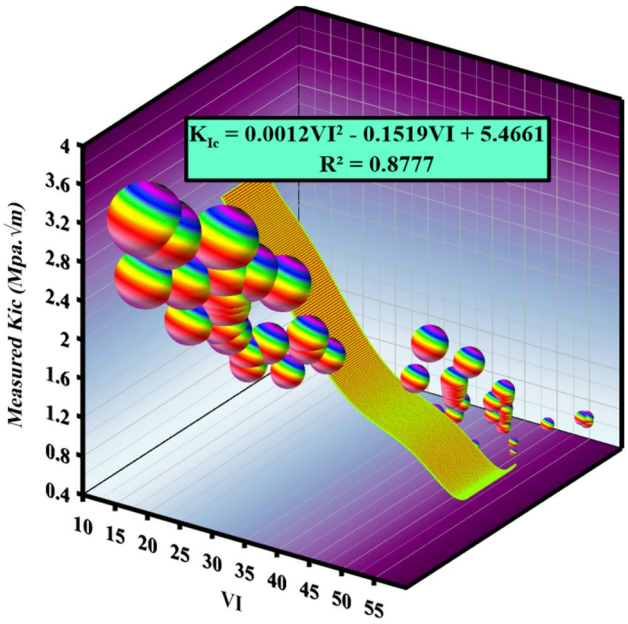

Fig. 11 The chart K_{Ic}-VI

After finding VI values for all input parameters, polynomial regression analysis was performed using Eq. (23) to build the model. Figure 11 demonstrates that the coefficient of determination (R^2) of 0.877 indicates acceptable accuracy of the polynomial regression model constructed using the RES method. Hence, the relationship described by Eq. (23) can be utilized to estimate K_{Ic}.

$$K_{Ic} = 0.0012VI^2 - 0.1519VI + 5.4661 \tag{22}$$

Results and model performance evaluation

After constructing various regression models, Table 12 presents the predicted fracture toughness values for 18 data points using linear, polynomial, exponential, logarithmic, power regressions, and the RES-based model with real values.

Three statistical measures were utilized to evaluate the accuracy of each model: R^2, MSE, and RMSE. Higher R^2 values approaching 1, as well as lower MSE and RMSE values approaching 0, indicate that the model's predictions are close to the actual measurements and possess high accuracy (Fattahi et al. 2024, 2021; Fattahi and Hasanipanah 2021; Fattahi and Zandy Ilghani 2021). These statistical criteria can be defined using the following equations:

$$R^2 = 1 - \frac{\sum_{k=1}^{n} (t_k - \widehat{t_k})^2}{\sum_{k=1}^{n} t_k^2 \frac{\sum_{i=1}^{n} \widehat{t^2}}{n}} \tag{23}$$

$$\mathrm{MSE} = \frac{1}{n} \sum_{k=1}^{n} (t_k - \widehat{t}_k)^2 \tag{24}$$

$$\mathrm{RMSE} = \sqrt{\frac{1}{n} \sum_{k=1}^{n} (t_k - \widehat{t}_k)^2} \tag{25}$$

Within the mentioned equations, n signifies the total number of samples, t_k represents the actual value, and $\widehat{t}_k$ represents the forecasted value for the k^{th} observation. Table 13 provides the evaluation results of the constructed models for K_{Ic}, including linear, polynomial, exponential, power,

Table 12 Comparison of real and predicted values for different models

VI	Measured K_{Ic}	Predicted K_{Ic}					
		Logarithmic	Logarithmic	Polynomial	Exponential	Linear	RES
39.6551	1.4	1.3128641	1.3128641	2.5096971	1.37	2.18639	1.329518
39.6551	1.63	1.2933195	1.2933195	2.5305435	1.50	2.11389	1.329518
36.2068	1.69	1.3834643	1.3834643	2.3756729	1.15	2.20685	1.539399
34.0517	1.73	2.0928639	2.0928639	2.5299412	1.98	2.48157	1.685067
35.7758	1.7	2.5524695	2.5524695	0.648371	2.34	2.78635	1.567641
32.3275	1.92	2.5524695	2.5524695	0.648371	2.34	2.78635	1.809627
28.4482	2.12	2.5524695	2.5524695	2.1832488	2.34	2.78635	2.115972
39.6551	1.44	1.3437478	1.3437478	2.4647072	1.25	2.21896	1.329518
45.2586	1.12	1.1116902	1.1116902	1.2243328	1.10	1.79237	1.049326
48.7068	1.003	1.1348119	1.1348119	1.1405632	1.32	1.6082	0.914356

Table 13 Evaluation and validation of the models

Model	MSE	RMSE	R^2	Observations
Power	0.01212	0.1101	0.8281	18
Linear	0.03386	0.184	0.7999	18
Logarithmic	0.04307	0.20755	0.6788	18
Exponential	0.12405	0.35221	0.2592	18
Polynomial	0.10666	0.32659	0.3452	18
RES	0.00819	0.0905	0.9659	18

logarithmic, and RES-based regression models. The RES-based model demonstrates significantly higher accuracy with $R^2 = 0.9659$, MSE = 0.00819, and RMSE = 0.0905 compared to other regression methods. The exponential and polynomial regression models exhibit high errors and substantial deviation from the real values.

To facilitate model evaluation, Fig. 12 presents a comparison chart between R^2 and RMSE for different models.

For a more comprehensive comparison of Table 12, Fig. 13 depicts the measured and predicted values of K_{Ic} using logarithmic, linear, polynomial, exponential, power, and RES-based regression models. for the 18 data points (model evaluation). As evident from the graph, the values obtained from the polynomial and exponential models significantly deviate from the actual values and the RES-based method.

As evidenced by both graphs and statistical metrics, the RES-based model showcases superior accuracy when compared to traditional regression methods. Nevertheless, given the multitude of forecasting models employing various regression techniques, the clarity of visual representation may be compromised in Table 12. Thus, Fig. 14 (bar chart) provides a more effective comparison of values obtained using the RES method with actual values across 18 data points. The graph underscores the close proximity and minimal disparity between predicted and actual values. Therefore, the polynomial equation derived from the RES method can be effectively applied in rock and mineral mechanics projects involving K_{Ic}.

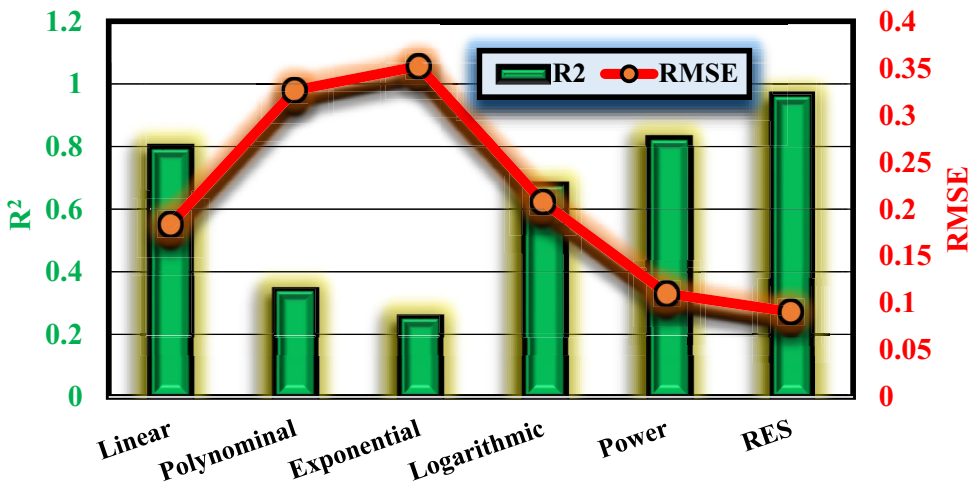

Fig. 12 Results and RMSE and R^2 statistical performance for all created models

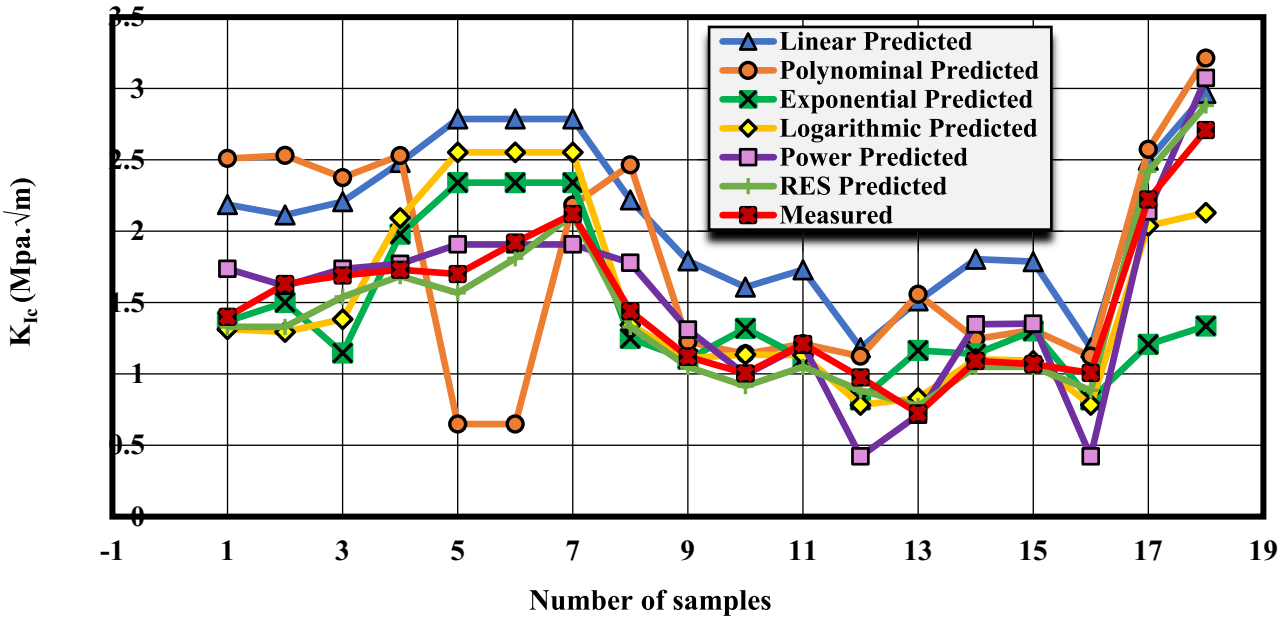

Fig. 13 Comparison between measured and predicted K_{Ic} values using various models

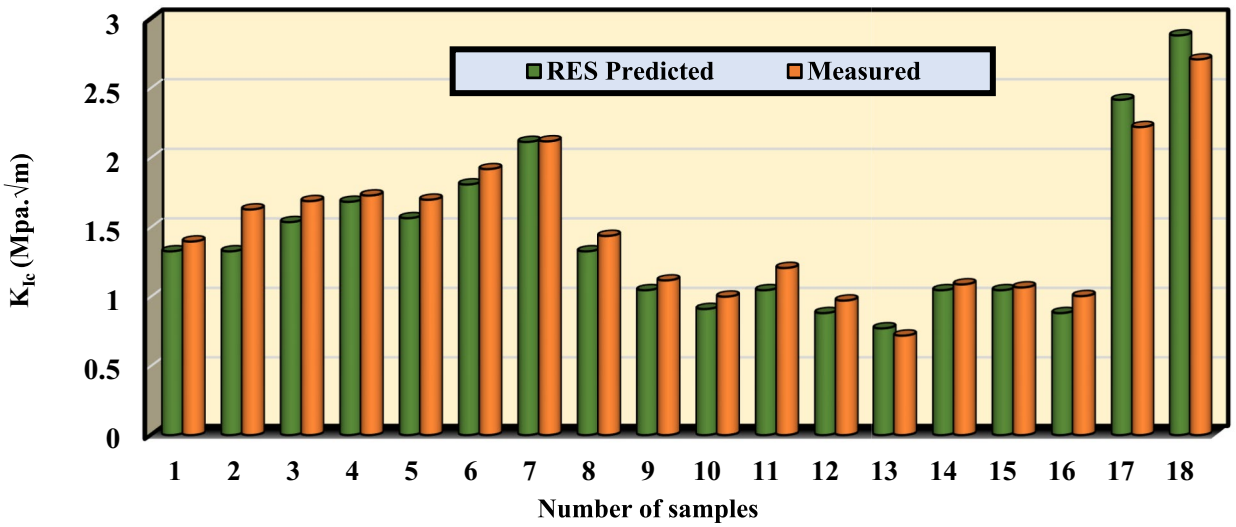

Fig. 14 **Comparison of predicted and actual K_{Ic} values based on the RES method**

Sensitivity analysis

Sensitivity Analysis (SA) is a crucial technique used across various fields of analysis and modeling to identify key parameters that significantly influence system behavior. By systematically varying one parameter while keeping others constant, SA reveals which inputs have the greatest impact on model outputs. This approach is invaluable for understanding complex relationships between input parameters and resulting outcomes, such as K_{Ic} values. In the study mentioned, SA was meticulously conducted on a K_{Ic} prediction model developed using the RES method. The goal was to assess the specific effects of input parameters— σ_t, α_0, R, α_B, B, and α_1 —on the accuracy of K_{Ic} predictions. @RISK software and Excel were employed for this purpose, with results detailed in Fig. 15. This analysis clearly illustrates how each parameter distinctly affects the model predictions based on the RES method. According to the sensitivity analysis, σ_t emerges as the most influential parameter, while B has the least impact on the K_{Ic} prediction model. Small fluctuations in σt significantly alter

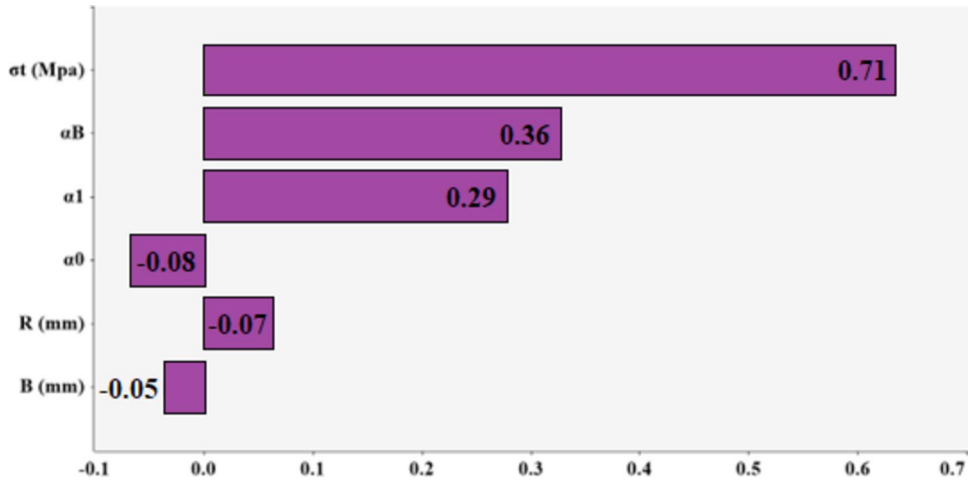

Fig. 15 The results of SA conducted for the developed model using the RES-based method

predicted K_{Ic} values, underscoring its critical role in governing model behavior. This finding suggests that focusing on σt, particularly its uniaxial compressive strength aspect, is crucial for engineers and practitioners involved in K_{Ic} -related studies. Such focused attention can optimize project outcomes by maximizing quality while minimizing costs and time investments.

Limitations and future works

The focus of this study was on predicting and estimating the fracture toughness of rock structures based on parameters such as disc radius, thickness, crack characteristics, and tensile strength. However, it is crucial to note that additional parameters, including uniaxial compressive strength, bending stress, modulus of elasticity, and Poisson's ratio, are also significant and warrant further investigation in future studies. Addressing these parameters could enhance the accuracy and applicability of fracture toughness models. In terms of modeling and addressing uncertainty, future research could explore the integration of intelligent methods alongside the RES method to compare and refine fracture toughness estimations for rock structures. This approach would contribute to advancing the understanding and predictive capabilities of such models. The RES method, leveraging expert opinions in rock engineering, demonstrates versatility across different rock types and geological conditions. Its high flexibility allows for application across various rock types, highlighting its potential for generalization in K_{Ic} predictions beyond specific rock types. However, a limitation of the RES method lies in the variability of expert opinions and their rankings when creating the effect matrix. Inconsistencies among experts can impact the accuracy and reliability of the analysis results. Moving forward, efforts should focus on standardizing expert inputs and addressing discrepancies to ensure robust and reliable application of the RES method in future studies across diverse geological contexts.

Discussion

The precise estimation of K_{Ic} in rock structures is pivotal for evaluating their stability and predicting crack propagation. This study conducted a comparison of various methods for predicting K_{Ic}, focusing on evaluating the effectiveness of the RES method. The RES method offers distinct advantages, including cost-effectiveness, simplicity, and the capability to accommodate uncertainties in rock parameters. The analysis concentrated on CCNBD samples, chosen for their ease of preparation in laboratory settings. Key input parameters considered in the study encompassed σ_t, R, B, α_B, α_0 and α_1. Using the RES method, a model was developed based on 70 data points, with an additional 18 points reserved for model evaluation. The accuracy of the RES-based model was assessed through comparison with alternative regression analysis methods, using metrics such as R^2, MSE, and RMSE. The results clearly showed that the RES-based method outperformed other regression techniques in predicting K_{Ic} for CCNBD samples, as evidenced by a higher R^2 value, indicating a stronger correlation between predicted and actual values. Moreover, the RES-based model exhibited lower MSE and RMSE values, indicating reduced deviation from actual values. Specifically, the RES-based model yielded an R^2 value of 0.9659, an MSE of 0.00819, and an RMSE of 0.0905, underscoring its superior accuracy compared to polynomial and exponential regression models, which showed higher errors and larger deviations. Continuing the study, sensitivity analysis was performed to identify the parameter most influencing the model's output. @RISK software facilitated this analysis, revealing that the parameter

σ_t exerted the greatest impact on the model's predictions. This finding underscores the sensitivity of model outcomes to variations in σ_t and emphasizes its crucial role in shaping predictions related to concrete structure growth and crack prevention. The RES method's strengths include its ability to handle uncertainties in rock parameters effectively, its cost-effectiveness, and its straightforward implementation. Furthermore, the study highlighted additional benefits of the RES method, including its capability to construct accurate, complex, and nonlinear models without necessitating intricate coding. This positions the RES method as a robust solution for accurately estimating fracture toughness in rock structures.

Conclusions

The RES method proves to be a highly reliable tool in this study for estimating and mitigating challenges within rock engineering, taking into account inherent uncertainties in rock properties. Its application facilitates the evaluation of fracture toughness in rock structures, thereby supporting informed decision-making and streamlining operations in mining and construction. The findings underscore the broader implications of the RES method in rock engineering, demonstrating its versatility across various rock types and geological conditions where input parameters align closely. However, differing geological contexts may necessitate tailored modeling approaches. Integrating the RES method into rock mechanics projects enhances precision, minimizes errors, and promotes timely project completion. Ultimately, the RES method emerges as a preferred approach over traditional regression methods due to its effectiveness, cost-efficiency, and ability to handle uncertainty. Its adoption promises significant advancements in mining engineering, geotechnics, and rock mechanics by overcoming conventional method limitations. These insights and outcomes provide valuable guidance for mining engineers and industry stakeholders, aiming to enhance safety, efficiency, and cost-effectiveness in mining and construction endeavors.

Funding Open Access funding enabled and organized by CAUL and its Member Institutions.

Data Availability To reproduce the simulations in the present study, the corresponding files can be found in Wang et al. (2021).

Declarations

Ethical approval This study does not contain any studies with human participants or animals performed by any of the authors.

Informed consent Informed consent was obtained from all individual participants included in the study.

Conflict of interest The authors declare that they have no conflict of interest.

References

Abe H, Keer L, Mura T (1976) Growth rate of a penny-shaped crack in hydraulic fracturing of rocks, 2. J Geophys Res 81:6292–6298

Afrasiabian B, Eftekhari M (2022) Prediction of mode I fracture toughness of rock using linear multiple regression and gene expression programming Journal of Rock Mechanics and Geotechnical. Engineering 14:1421–1432

Aliha M, Ayatollahi M (2014) Rock fracture toughness study using cracked chevron notched Brazilian disc specimen under pure modes I and II loading–A statistical approach. Theor Appl Fract Mech 69:17–25

Aliha M, Ashtari R, Ayatollahi MR (2006) Mode I and mode II fracture toughness testing for a coarse grain marble. Applied mechanics and materials. Trans Tech Publ, pp 181–188

Aliha M, Mahdavi E, Ayatollahi M (2018) Statistical analysis of rock fracture toughness data obtained from different chevron notched and straight cracked mode I specimens. Rock Mech Rock Eng 51:2095–2114

Alkılıçgil Ç (2006) Development of a new method for mode I fracture toughness test on disc type rock specimens. M.S. - Master of Science. Middle East Technical University

Ayatollahi M, Akbardoost J (2014) Size and Geometry Effects on Rock Fracture Toughness: Mode I Fracture. Rock Mech Rock Eng 47:677–687

Bearman R (1999) The use of the point load test for the rapid estimation of Mode I fracture toughness. Int J Rock Mech Min Sci 36:257–263

Benardos A, Kaliampakos D (2004) A methodology for assessing geotechnical hazards for TBM tunnelling—illustrated by the Athens Metro Greece. Int J Rock Mech Min Sci 41:987–999

Bhagat RB (1985) Mode I fracture toughness of coal Int J Min Eng 3:229–236. https://doi.org/10.1007/BF00880769

Chong KP, Kuruppu MD, Kuszmaul JS (1987) Fracture toughness determination of layered materials. Eng Fract Mech 28:43–54

Cui Z-d, Liu D-a, An G-m, Sun B, Zhou M, Cao F-q (2010) A comparison of two ISRM suggested chevron notched specimens for testing mode-I rock fracture toughness Int J Rock Mech Min Sci 47:871-876

Daghigh V, Lacy TE Jr, Daghigh H, Gu G, Baghaei KT, Horstemeyer MF, Pittman CU Jr (2020) Machine learning predictions on fracture toughness of multiscale bio-nano-composites. J Reinf Plast Compos 39:587–598

Dehestani A, Kazemi F, Abdi R, Nitka M (2022) Prediction of fracture toughness in fibre-reinforced concrete, mortar, and rocks using various machine learning techniques. Eng Fract Mech 276:108914

Emami Meybodi E, Hussain SK, Fatehi Marji M, Rasouli V (2022) Application of Machine Learning Models for Predicting Rock Fracture Toughness Mode-I and Mode-II. J Min Environ 13:465–480

Fakhri D, Khodayari A, Mahmoodzadeh A, Hosseini M, Ibrahim HH, Mohammed AH (2022) Prediction of Mixed-mode I and II effective fracture toughness of several types of concrete using the extreme gradient boosting method and metaheuristic optimization algorithms. Eng Fract Mech 276:108916

Fattahi H (2017) Risk Assessment and Prediction of Safety Factor for Circular Failure Slope Using Rock Engineering Systems. Environ Earth Sci 76:224

Fattahi H, Babanouri N (2018) RES-Based Model in Evaluation of Surface Settlement Caused by EPB Shield Tunneling. Indian Geotech J 48:746–752

Fattahi H, Hasanipanah M (2021) An indirect measurement of rock tensile strength through optimized relevance vector regression models, a case study. Environ Earth Sci 80:748. https://doi.org/10.1007/s12665-021-10049-2

Fattahi H, Moradi A (2018) A New Approach for Estimation of the Rock Mass Deformation Modulus: a Rock Engineering Systems-Based Model. Bull Eng Geol Environ 77:363–374

Fattahi H, Zandy Ilghani N (2021) Hybrid wavelet transform with artificial neural network for forecasting of shear wave velocity from wireline log data: a case study. Environ Earth Sci 80:5. https://doi.org/10.1007/s12665-020-09320-9

Fattahi H, Hasanipanah M, Zandy Ilghani N (2021) Investigating Correlation of Physico-Mechanical Parameters and P-Wave Velocity of Rocks: a Comparative Intelligent Study. J Min Environ 12:863–875. https://doi.org/10.22044/jme.2021.11121.2092

Fattahi H, Ghaedi H, Malekmahmoodi F (2024) Prediction of rock drillability using gray wolf optimization and teaching–learning-based optimization techniques. Soft Comput 28:461–476. https://doi.org/10.1007/s00500-023-08233-6

Fowell R (1995) ISRM commission on testing methods. Suggested method for determining mode I fracture toughness using cracked chevron notched Brazilian disc (CCNBD) specimens. Int J Rock Mech Min Sci Geomech Abstr 32:57–64

Fowell R, Hudson J, Xu C, Zhao X (1995) Suggested method for determining mode I fracture toughness using cracked chevron notched Brazilian disc (CCNBD) specimens. In Int J Rock Mech Mining Sci Geomechanics Abstracts 32:322A

Fowell R, Xu C (1993) The cracked chevron notched Brazilian disc test-geometrical considerations for practical rock fracture toughness measurement. In: International journal of rock mechanics and mining sciences & geomechanics abstracts, 7. Pergamon, 821–824

Fowell R, Xu C, Dowd P (2006) An update on the fracture toughness testing methods related to the cracked chevron-notched Brazilian disk (CCNBD) specimen. Pure Appl Geophys 163:1047–1057

Frough O, Torabi SR (2013) An application of rock engineering systems for estimating TBM downtimes. Eng Geol 157:112–123

Funatsu T, Shimizu N, Kuruppu M, Matsui K (2015) Evaluation of mode I fracture toughness assisted by the numerical determination of K-resistance. Rock Mech Rock Eng 48:143–157

Ghanbari K, Ataei M, Sereshki F, Saffari A (2018) Determination and Assessment of Coal Bed Methane Potential Using Rock Engineering Systems. J Min Environ 9:605–621

Hamdia KM, Lahmer T, Nguyen-Thoi T, Rabczuk T (2015) Predicting the fracture toughness of PNCs: A stochastic approach based on ANN and ANFIS. Comput Mater Sci 102:304–313

Hasanipanah M, Jahed Armaghani D, Monjezi M, Shams S (2016) Risk assessment and prediction of rock fragmentation produced by blasting operation: a rock engineering system. Environ Earth Sci 75:1–12

Hudson JA (1992) Rock engineering systems: Theory and practice. Ellis Horwood

Kuruppu MD, Obara Y, Ayatollahi MR, Chong K, Funatsu T (2014) ISRM-suggested method for determining the mode I static fracture toughness using semi-circular bend specimen. Rock Mech Rock Eng 47:267–274

Lim I, Johnston I, Choi S (1994) Boland J Fracture testing of a soft rock with semi-circular specimens under three-point bending. Part 1—mode I. In Int J Rock Mech Min Sci Geomechanics Abstracts, 3. Elsevier 185–197

Liu G, Zhong Z, Ye T, Meng J, Zhao S, Liu J, Luo S (2024) Impact failure and disaster processes associated with rockfalls based on three-dimensional discontinuous deformation analysis. Earth Surf Process Landf 49(11):3344–66

Liu G, Meng H, Song G, Bo W, Zhao P, Ning B, Xu X (2024) Numerical simulation of wedge failure of rock slopes using three-dimensional discontinuous deformation analysis. Environ Earth Sci 83:310

Ma K, Yuan F, Wang H, Zhang Z, Sun X, Peng Y, Wang H (2021) Fracture mechanism of roof key strata in Dongjiahe coal mine using microseismic moment tensor Geomatics. Nat Haz Risk 12:1467–1487

Ma K, Liu G (2022) Three-dimensional discontinuous deformation analysis of failure mechanisms and movement characteristics of slope rockfalls. Rock Mech Rock Eng 55:275–296. https://doi.org/10.1007/s00603-021-02656-z

Mahmoodzadeh A, Nejati HR, Mohammadi M, Ibrahim HH, Khishe M, Rashidi S, Ali HFH (2022) Prediction of Mode-I rock fracture toughness using support vector regression with metaheuristic optimization algorithms. Eng Fract Mech 264:108334

Mahmoodzadeh A, Fakhri D, Mohammed AH, Mohammed AS, Ibrahim HH, Rashidi S (2023) Estimating the effective fracture toughness of a variety of materials using several machine learning models. Eng Fract Mech 286:109321

Mazhnik E, Oganov AR (2020) Application of machine learning methods for predicting new superhard materials. J Appl Phys 128:075102

Mohammadi H, Azad A (2021) Prediction of ground settlement and the corresponding risk induced by tunneling: An application of rock engineering system paradigm. Tunn Undergr Space Technol 110:103828

Mohammadi S (2008) Extended finite element method: for fracture analysis of structures. John Wiley & Sons

Ouchterlony F (1981) Extension of the compliance and stress intensity formulas for the single edge crack round bar in bending. ASTM International. https://doi.org/10.1520/STP28309S

Preiß E (2018) Fracture toughness of freestanding metallic thin films studied by bulge testing. FAU University Press. https://doi.org/10.25593/978-3-96147-118-8

Roy DG, Singh T, Kodikara J (2018) Predicting mode-I fracture toughness of rocks using soft computing and multiple regression. Measurement 126:231–241

Saffari A, Sereshki F, Ataei M, Ghanbari K (2013) Applying rock engineering systems (RES) approach to evaluate and classify the coal spontaneous combustion potential in Eastern Alborz coal mines. Int J Min Geo-Eng 47:115–127

Saouma V (2000) Fracture Mechanics. Lecture Notes Dept of Civil Environmental and Architectural Engineering, University of Colorado, Boulder, USA

Schmidt R, Huddle C (1977) Effect of confining pressure on fracture toughness of Indiana limestone. In: International Journal of Rock Mechanics and Mining Sciences & Geomechanics Abstracts 5–6. Elsevier, 289–293

Seber GA, Lee AJ (2003) Linear regression analysis, vol 330. John Wiley & Sons. https://doi.org/10.1002/9780471722199

Sun Z, Ouchterlony F (1986) Fracture toughness of Stripa granite cores. In: International Journal of Rock Mechanics and Mining Sciences & Geomechanics Abstracts, 6. Elsevier, 399–409

Tutluoglu L, Keles C (2011) Mode I fracture toughness determination with straight notched disk bending method. Int J Rock Mech Min Sci 48:1248–1261

Wang Y-T, Zhang X, Liu X-S (2021) Machine learning approaches to rock fracture mechanics problems: Mode-I fracture toughness determination. Eng Fract Mech 253:107890

Wei M, Dai F, Xu N, Zhao T (2018a) Experimental and numerical investigation of cracked chevron notched Brazilian disc specimen for fracture toughness testing of rock. Fatigue Fract Eng Mater Struct 41:197–211

Wei MD, Dai F, Liu Y, Xu NW, Zhao T (2018b) An experimental and theoretical comparison of CCNBD and CCNSCB specimens for determining mode I fracture toughness of rocks. Fatigue Fract Eng Mater Struct 41:1002–1018

Wu H, Kemeny J, Wu S (2017) Experimental and numerical investigation of the punch-through shear test for mode II fracture toughness determination in rock. Eng Fract Mech 184:59–74

Xu Y, Dai F, Zhao T, Xu N-w, Liu Y (2016) Fracture toughness determination of cracked chevron notched Brazilian disc rock specimen via Griffith energy criterion incorporating realistic fracture profiles. Rock Mech Rock Eng 49:3083–3093

Zhou Q, Herrera J, Hidalgo A (2019) Development of a quantitative assessment approach for the coal and gas outbursts in coal mines using rock engineering systems. Int J Min Reclam Environ 33:21–41